

Electronic Supplementary Material (ESI) for Journal of Materials Chemistry A. This journal is © The Royal Society of Chemistry 2019

Supplementary Information

Nitrogen-Doped Hollow Carbon Nanosphere Towards Application of Potassium Ion Storage

Jiafeng Ruan,^{a,1} Xi Wu,^{a,1} Yan Wang,^a Shiyong Zheng,^b Dalin Sun,^a Yun Song,^{a,} Min Chen^{a,*}*

^a Department of Materials Science, Fudan University, Shanghai 200433 (P. R. China)

^b School of Materials Science and Engineering, University of Shanghai for Science and Technology, Shanghai 200093, China

*Corresponding author at: Department of Materials Science, Fudan University, Shanghai 200433 (P. R. China)

E-mail addresses: Chenmin@fudan.edu.cn; Songyun@fudan.edu.cn.

¹ These authors contributed equally to this work.

Content:

Figure S1. Zeta (ζ) potential of SiO₂-NH₂ and Si.

Figure S2. TEM image of the SiO₂-NH₂@DA/Si.

Figure S3. (a, b) TEM images of N-CNs.

Figure S4. (a) XRD pattern and (b) Raman spectra of N-CNs.

Figure S5. Raman spectra of the N-HCNs

Table S1. Assignments and percentage composition in the C1s and N 1s regions of the N-HCNs.

Figure S6. The SEM images of N-HCNs.

Figure S7. The SEM images of N-HCNs: (a) pristine and (b) after 100 cycles.

Figure S8. initial three discharge/charge profiles of N-CNs at 0.05 A g⁻¹

Figure S9. Initial two discharge/charge profiles of the N-HCNs based on the (a) cycle performance at 50 mA g⁻¹ and (b) rate performance at 50 mA g⁻¹.

Figure S10. Comparison of rate capability of the N-HCNs and other carbonaceous materials in PIB.

Figure S11. CV curve with the pseudocapacitive fraction shown by the red region at a scan rate of (a) 5.0 mV s⁻¹ and (b) 10.0 mV s⁻¹.

Figure S12. (e) Nyquist plots of N-HCNs at different potentials; (f) the liner relation of $\omega^{1/2}$ vs. $-Z''$.

Figure S13. Electrochemical performance of commercial TiS₂ as PIBs cathodes in half cells: (a) CV curves within the voltage window of 1.5-3.0 V at a scan rate of 0.1 mV s⁻¹; (b) initial three discharge/charge profiles at 0.1 A g⁻¹; (c) rate capability of at current rates of 0.05, 0.1, 0.2, 0.5, 1.0 and 2.0 A g⁻¹; (d) cycling property at 0.1 A g⁻¹.

Figure S14. initial GDC profile of full-cell at 0.1 A g⁻¹.

Figure S1

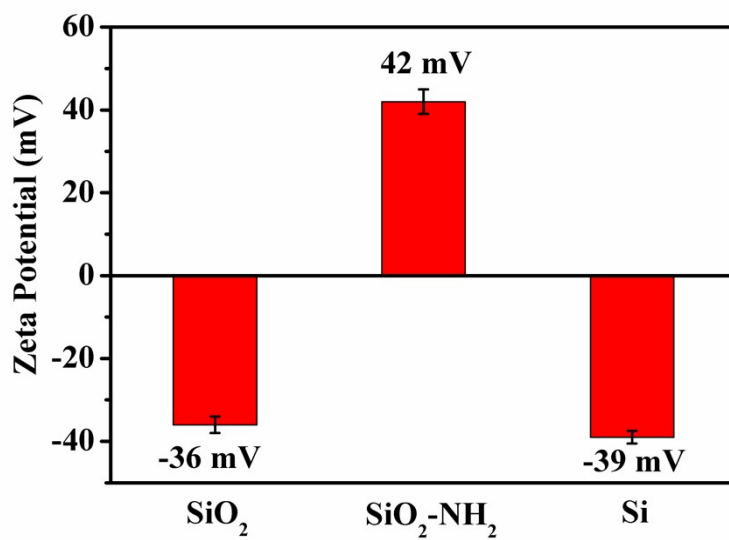


Figure S1. Zeta (ζ) potential of SiO₂-NH₂ and Si.

Figure S2

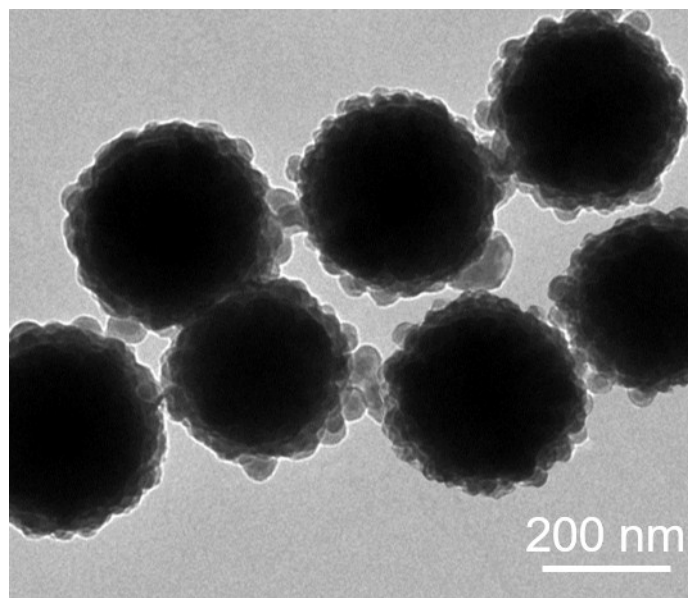


Figure S2. TEM image of the $\text{SiO}_2\text{-NH}_2\text{@DA/Si}$.

Figure S3

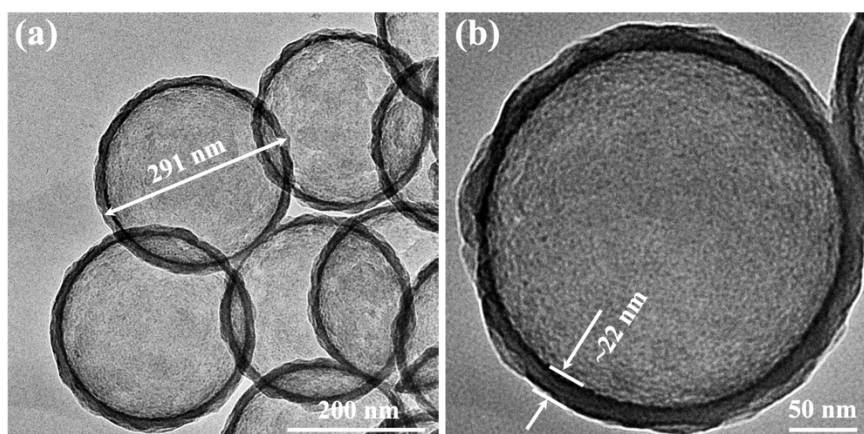


Figure S3. (a, b) TEM images of N-CNs.

Figure S4

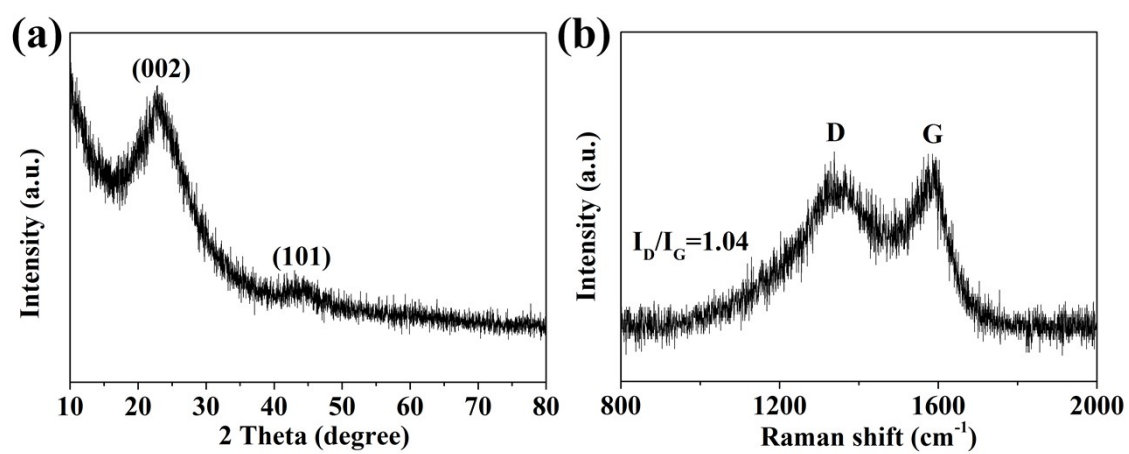


Figure S4. (a) XRD pattern and (b) Raman spectra of N-CNs.

Figure S5

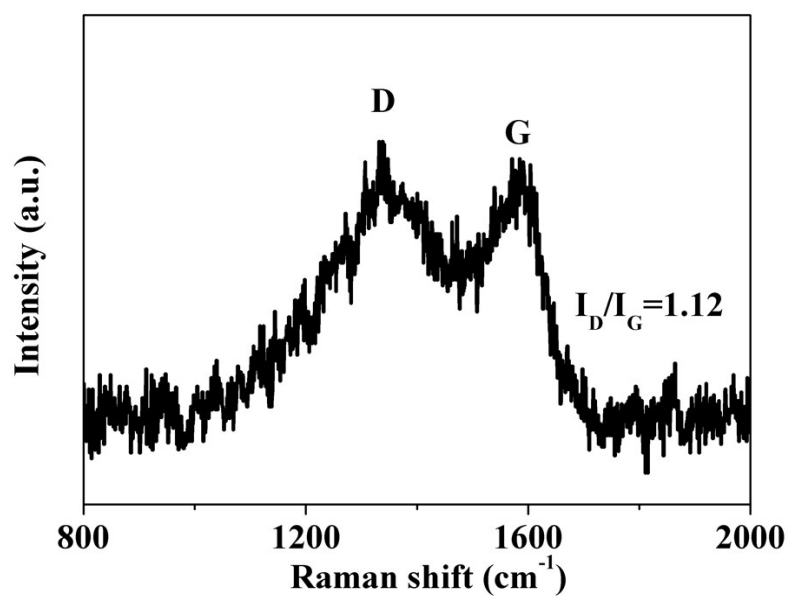


Figure S5. Raman spectra of the N-HCNs

Table S1**Table S1.** Assignments and percentage composition in the C 1s and N 1s regions of the N-

HCNs

	functional group	binding energy (eV)	ratios (%area)
C 1s	C-C sp ²	284.6	69.7
	C=N	286.1	23.6
	C-N/C-O-C	288.2	6.7
N 1s	pyridinic-N	398.6	53.4
	pyrrolic-N	400.0	22.6
	quaternary-N	401.0	24.0

Figure S6

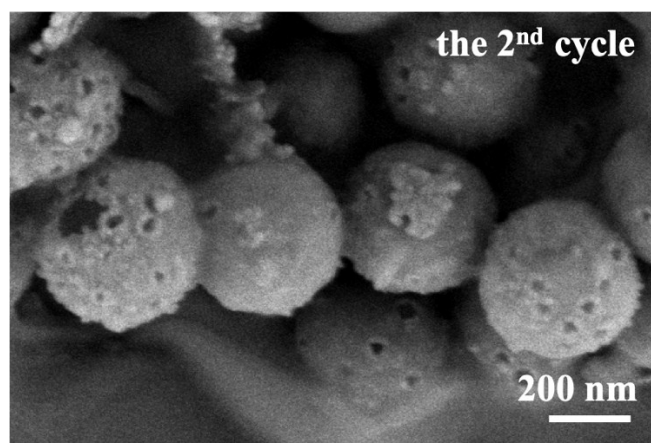


Figure S6. The SEM images of N-HCNs.

Figure S7

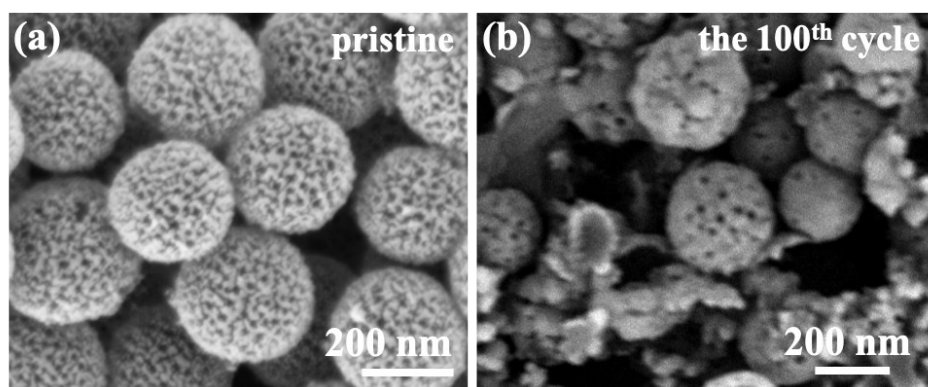


Figure S7. The SEM images of N-HCNs: (a) pristine and (b) after 100 cycles.

The morphology of the pristine and after cycling N-HCNs are carried out, as shown in Figure S7. As compared with the morphology of the pristine N-HCNs, there is no significant difference between before cycling and after cycling, except for the size of the pores. The change can be ascribed to the solid SEI on the surface of the N-HCNs, leading to low initial CE.

Figure S8

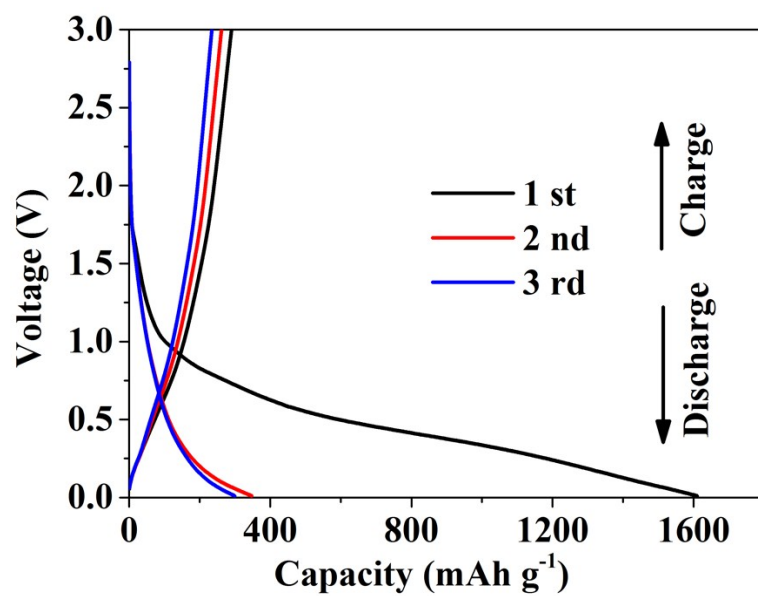


Figure S8. initial three discharge/charge profiles of N-CNs at 0.05 A g⁻¹

Figure S9

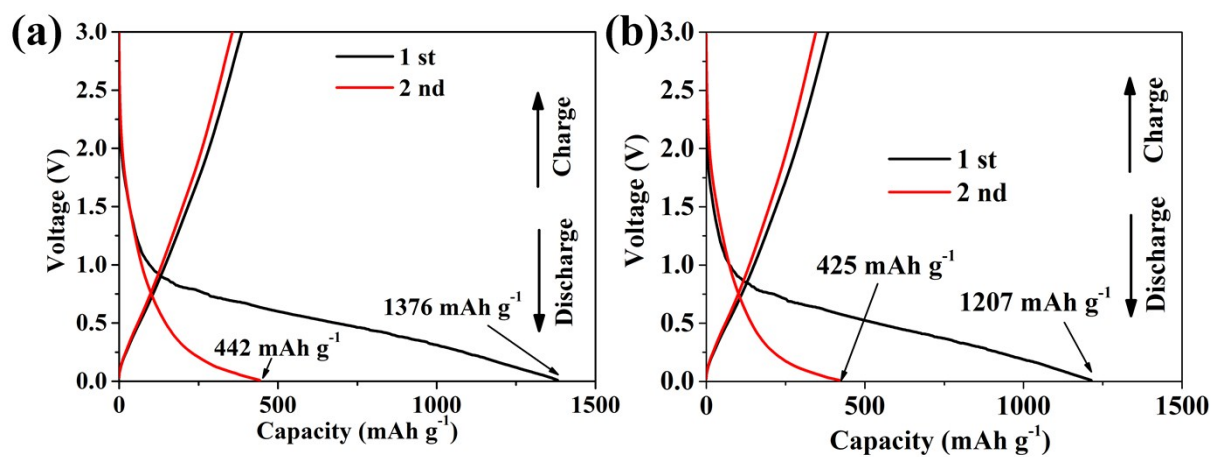


Figure S9. Initial two discharge/charge profiles of the N-HCNs based on the (a) cycle performance at 50 mA g^{-1} and (b) rate performance at 50 mA g^{-1} .

Figure S10

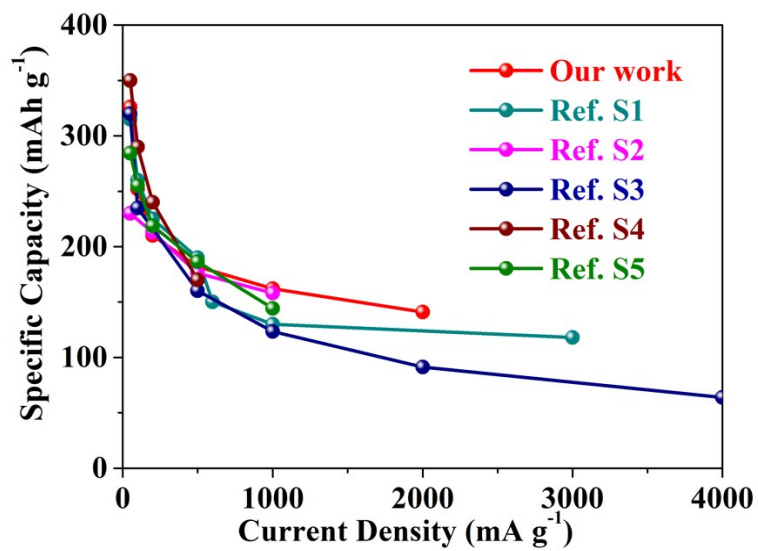


Figure S10. Comparison of rate capability of the N-HCNs and other carbonaceous materials in PIB.

Figure S11

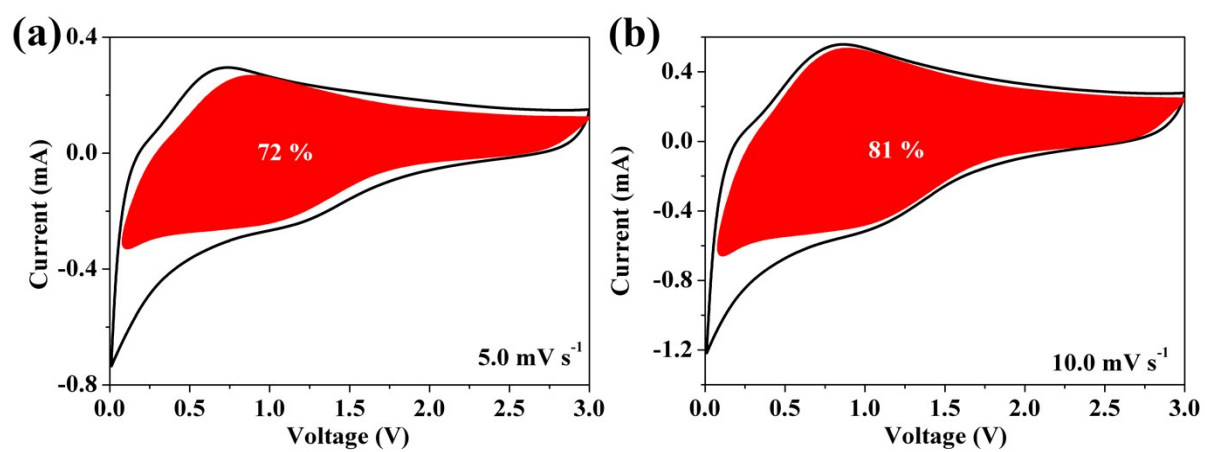


Figure S11. CV curve with the pseudocapacitive fraction shown by the red region at a scan rate of (a) 5.0 mV s⁻¹ and (a) 10.0 mV s⁻¹.

Figure S12

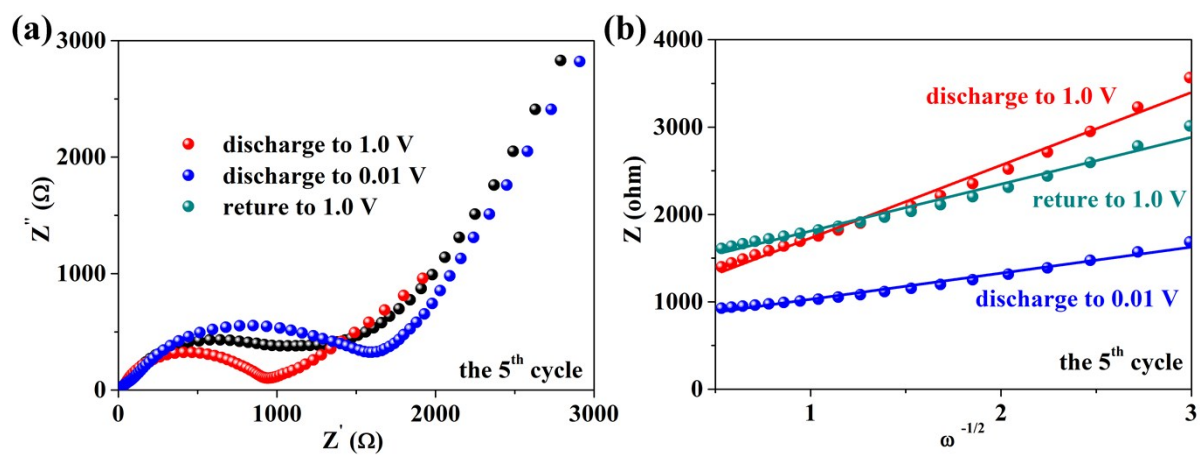


Figure S12. (e) Nyquist plots of N-HCNs at different potentials; (f) the linear relation of $\omega^{1/2}$ vs. $-Z''$.

Figure S13

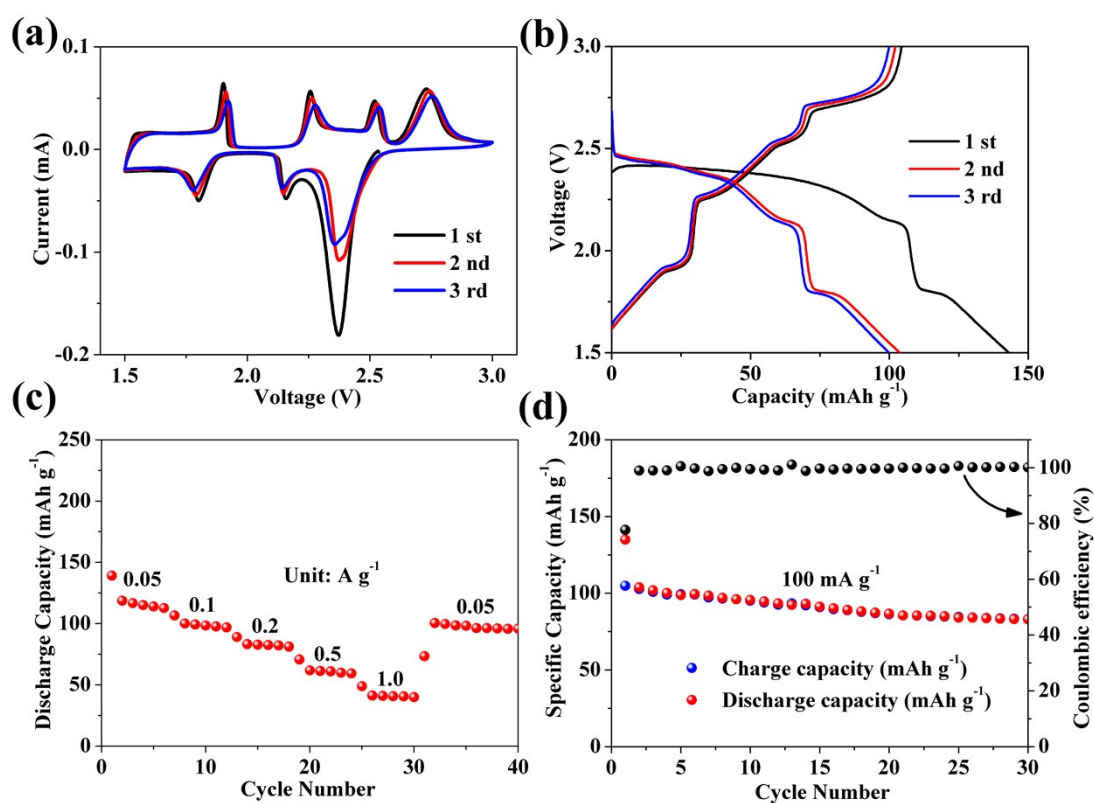


Figure S13. Electrochemical performance of commercial TiS_2 as PIBs cathodes in half cells: (a) CV curves within the voltage window of 1.5-3.0 V at a scan rate of 0.1 mV s^{-1} ; (b) initial three discharge/charge profiles at 0.1 A g^{-1} ; (c) rate capability of at current rates of 0.05, 0.1, 0.2, 0.5, 1.0 and 2.0 A g^{-1} ; (d) cycling property at 0.1 A g^{-1} .

Figure S14

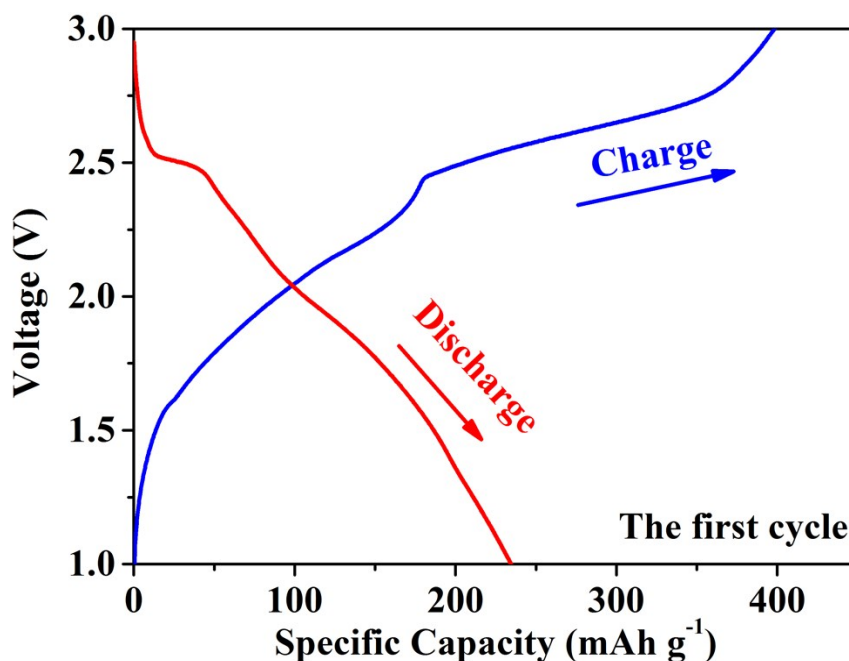


Figure S14. initial GDC profile of full-cell at 0.1 A g⁻¹

Reference:

- [S1] J. Yang, Z. Ju, Y. Jiang, Z. Xing, B. Xi, J. Feng, S. Xiong, Enhanced Capacity and Rate Capability of Nitrogen/Oxygen Dual-Doped Hard Carbon in Capacitive Potassium-Ion Storage, *Adv. Mater.*, 30(2017)1700104. <https://doi.org/10.1002/adma.201700104>.
- [S2] M. Che, W. Wang, X. Liang, S. Gong, J. Liu, Q. Wang, S. Guo, H. Yang, Sulfur/Oxygen Codoped Porous Hard Carbon Microspheres for High-Performance Potassium-Ion Batteries, *Adv. Energy Mater.*, 8(2018)1800171. <https://doi.org/10.1002/aenm.201800171>.
- [S3] A. Mahmood, S. Li, Z. Ali, H. Tabassum, B. Zhu, Z. Liang, W. Meng, W. Aftab, W. Guo, H. Zhang, M. Yousaf, S. Gao, R. Zou, Y. Zhao, Ultrafast Sodium/Potassium-Ion Intercalation into Hierarchically Porous Thin Carbon Shells, *Adv. Mater.*, 31(2019) 1805430. <https://doi.org/10.1002/adma.201805430>.
- [S4] Z. Ju, P. Li, G. Ma, Z. Xing, Q. Zhuang, Y. Qian, Few Layer Nitrogen-Doped Graphene with Highly Reversible Potassium Storage, *Energy Storage Mater.*, 11(2018)38-46. <https://doi.org/10.1016/j.ensm.2017.09.009>.
- [S5] W. Wang, J. Zhou, Z. Wang, L. Zhao, P. Li, Y. Yang, C. Yang, H. Huang, S. Guo, Short-Range Order in Mesoporous Carbon Boosts Potassium-Ion Battery Performance, *Adv. Energy Mater.*, 8(2018)1701648. <https://doi.org/10.1002/aenm.201701648>.